Directional Spectrum Estimation for Sea States Generated by the Single Summation Method

Iversen, Sarah Krogh; Andersen, Thomas Lykke; Frigaard, Peter

Published in:
CoastLab 2024

DOI (link to publication from Publisher):
10.59490/coastlab.2024.693

Publication date:
2024

Document Version
Publisher's PDF, also known as Version of record

Proceedings of the 9th International Conference on Physical Modelling in Coastal Engineering (Coastlab24)
Delft, Netherlands, May 13-16, 2024

Conference Paper, DOI: 10.59490/coastlab.2024.693

DIRECTIONAL SPECTRUM ESTIMATION FOR SEA STATES GENERATED BY THE SINGLE SUMMATION METHOD

SARAH KROGH IVERSEN[1], THOMAS LYKKE ANDERSEN[2], PETER FRIGAARD[3]

1 Dept. of the Built Environment, Aalborg University, Denmark, ski@build.aau.dk
2 Dept. of the Built Environment, Aalborg University, Denmark, tla@build.aau.dk
3 Dept. of the Built Environment, Aalborg University, Denmark, pf@build.aau.dk

ABSTRACT

The influence of directional spreading of waves is significant for wave-induced loads, wave breaking and nonlinearity of the waves. For physical model testing performed at test facilities such as the Ocean and Coastal Engineering Laboratory at Aalborg University, it is crucial to validate if the test conditions match the target sea states by measurement and analysis of the generated directional wave field. Most of the existing methods assumes a double summation sea state to be present which is valid in the prototype. However, waves in the laboratory are usually generated by single summation. The current paper presents a method to analyse short-crested waves generated by the single summation method. Compared to similar methods oblique reflections are considered instead of only in-line reflections. The results show that the method successfully decomposes the incident and reflected wave fields in the time domain. Thus, for example the incident wave height distribution may be obtained. The sensitivity of the new method to additional reflective directions, noise, calibration errors and positional errors of the wave gauges was found small.

KEYWORDS: Wave Analysis, Directional Spectrum Estimation, Directional Spreading Function, Single Summation Method, Wave Reflection

1 INTRODUCTION

In design of coastal and offshore structures, the directionality of the waves is important to consider. The directionality of the waves will influence the wave kinematics, the loads on the structures, the wave breaking, the nonlinearity of the waves and the likelihood of extreme waves. For design of wave energy converters, the directionality might also influence the power production significantly depending on the type of device. A widely used tool in design of coastal and offshore structures is physical model testing in wave tank facilities. Analysis of the generated multidirectional wave field in the model is needed to validate that the target sea states are obtained.

For physical model testing it is common to analyse the short-crested waves from measurements of surface elevation time series in multiple positions. Most existing methods for directional spectrum estimation aim to solve the Directional Spreading Function (DSF) and cover the commonly applied methods; BDM (Hashimoto & Kobune, 1988), MLM ((Capon *et al.*, 1976), (Isobe *et al.* 1984) and (Krogstad, 1988)) and MEM (Hashimoto *et al.*, 1994). The DSF-based reconstruction methods assume that the wave field is generated by double summation, which means that many directions will be present at each frequency. This will be the case in a natural environment, but for laboratory tests Miles and Funke (1989) recommended to use single summation generation. This means that each frequency has just one generated direction of propagation. Their recommendation was based on the requirement to have a spatially homogeneous incident energy level in the basin.

A comparative analysis of different analysis methods for short-crested waves was performed in Hawkes *et al.* (1997), from which it was concluded that most of the methods does not detect the reflected wave components very well. Especially for wave fields close to the reflecting structure, where phase-locking will occur. Moreover, most of the methods assume that the DSF is either of a specific shape or at least that it is a smooth function, which is not necessarily the case. For laboratory generated waves the spreading function has to be truncated as otherwise too large spurious waves will be generated due to the discretization of the wavemaker. Moreover, single summation generated sea states do not necessarily have a smooth DSF within each frequency bin analysed.

When analysing waves in physical model tests, a time domain solution providing the incident wave train is often desired. This is because the response of the structure is usually characterized by time domain parameters including for example H_{max}, $H_{2\%}$ and $H_{1/3}$. The aforementioned methods only provide spectral parameters. Another type of method will be considered in the present work, which will allow for a decomposition in the time domain by utilizing the knowledge that a single summation sea state is present. Thus, exactly the frequencies generated are analysed and therefore the resolution of the analysed frequency domain is equal to the one used for generation. For a wave field generated by single summation, this will mean that only a single incident direction is present at each generated frequency. It is important to note that analysis of exactly the frequencies generated require synchronization of the wave generation and acquisition to avoid influence of crystal clock differences. Draycott *et al.* (2016) showed that the combined wave generation-measurement approach used in the SPAIR method enables increased certainty in estimation of the directional spectra compared to the DSF-based reconstruction methods, that are inherently associated with some uncertainty. In the SPAIR method by Draycott *et al.* (2016) an incident wave component is assumed to give rise to a single reflected component in the opposite direction. This is certainly not always valid but is valid for a circular wave basin without a structure for which the SPAIR method was developed. The assumption of in-line reflection allow for the separation of the incident and reflected waves using methods developed for long-crested waves, i.e. Zelt and Skjelbreia (1993), Goda and Suzuki (1976) or Mansard and Funke (1980). For structures exposed to short-crested waves, the reflected direction is in many cases unknown. When oblique reflections occur, fitting initially to a single direction as done in the SPAIR method will lead to wrong estimation of the direction. The present paper will therefore present a method to perform the decomposition in incident and reflected components independent of the directional difference between the two. The new method is named SORS, Single-summation Oblique Reflection Separation.

The method requires the generated incident wave field to be of the single summation model. This will usually yield just one incident and one reflected direction for each frequency component. Other components may though be present due to corner reflection compensation (Dalrymple, 1989), diffraction from one or more models, cross-modes, wall reflections, and nonlinear interactions in the sub and superharmonic regions. Common for the different contributions is, that they diverge from the single summation model assumptions and are therefore not considered in the mathematical model. Apart from that also calibration errors and measurement uncertainties and noise could be present in the signals. In the present work it will therefore be tested how sensitive the wave decomposition is towards such phenomena. First, the methodology of the present work will be presented including wave generation and the principles of the method. Next, the sensitivity towards diverging factors will be tested by synthetically generated data. Here it will be presented by the influence on the estimated incident and reflected time series. Finally, the stability of the method is shortly discussed along with future development of the method.

2 THE NEW SORS METHOD

The use of the SORS method assumes that the wave field is generated from the single summation method by linear wave theory as expressed in Eq. (1), where a_i is the amplitude, k_i is the wave number, θ_i is the direction of propagation, ω_i is the angular frequency and ϕ_i is the phase shift, all of them of the i'th wave component for $i = 0, 1, \dots N-1$, where N is the total number of frequency components.

$$\eta(x,y,t) = \sum_{i=0}^{N-1} a_i \cos[k_i(x\cos\theta_i + y\sin\theta_i) - \omega_i t + \varphi_i] \tag{1}$$

It is assumed that there is no interaction between the wave components. It is furthermore assumed that the wave field is stationary, that no wave breaking or shoaling occurs, and that each angular frequency ($\omega_i = 2\pi f_i$) has just one incident and one reflected wave component, that are not necessarily in line with each other. The frequencies in the signal are assumed known from the wave generation (N frequencies, $f_i = i \cdot \Delta f, i = 1, 2 \dots N-1, \Delta f = \frac{f_s}{N}$). Acquisition and wave generation needs to be synchronized to avoid differences in sample frequencies (f_s) caused by crystal clock variations.

The surface elevation of irregular three-dimensional waves including incident and reflected wave components in position (x, y) can then be described by:

$$\eta(x,y,t) = \sum_{i=0}^{N-1} a_{I,i} \cos\left[k_i\left(x\cos\theta_{I,i} + y\sin\theta_{I,i}\right) - \omega_i t + \varphi_{I,i}\right] + \sum_{i=0}^{N-1} a_{R,i} \cos\left[k_i\left(x\cos\theta_{R,i} + y\sin\theta_{R,i}\right) - \omega_i t + \varphi_{R,i}\right] + \text{noise} \tag{2}$$

The wave number, k, is determined from the linear dispersion relation, where ω is the frequency of the wave component and h is the water depth.

$$\omega^2 = gk\tanh(kh) \tag{3}$$

The directional analysis is performed one frequency at a time, wherefore i is omitted in the following. The surface

elevation in frequency domain, $\hat{\eta}$, can then be described from Equation (4) at each gauge position m, where $m = 1,2 \ldots P$, for the total number of gauges, P.

$$\hat{\eta}(x_m, y_m) = C_{I,m}X_I + C_{R,m}X_R + \Omega_m \tag{4}$$
$$X_I = a_I \exp[-\mathrm{i}\varphi_I]$$
$$X_R = a_R \exp[-\mathrm{i}\varphi_R]$$
$$C_{I,m} = \exp[-\mathrm{i}k(x_m \cos\theta_I + y_m \sin\theta_I)]$$
$$C_{R,m} = \exp[-\mathrm{i}k(x_m \cos\theta_R + y_m \sin\theta_R)]$$

where Ω_m is the Fourier transformation of the noise at gauge m and frequency ω. C_I and C_R are here defined based on the absolute phases, wherefore X_I and X_R are the complex wave amplitude of the incident and reflected wave components respectively in position $(x,y) = (0,0)$. The values of the complex parameters, X_I and X_R are determined by fitting Equation (4) into the measurement at each frequency by minimising the sum of squares of Ω_m when summing over all gauge positions, which for the present implementation yields the total error, E, in Eq. (5).

$$E = \sum_m (\Omega_m)^2 = \sum_m \left(\hat{\eta}(x_m, y_m) - C_{I,m}X_I - C_{R,m}X_R\right)^2 \tag{5}$$

The total error, E, should be minimised with respect to the unknowns X_I , X_R , θ_I and θ_R. For a given estimate of θ_I and θ_R it can be minimised with respect to X_I and X_R respectively by:

$$\frac{\partial}{\partial X_I}\sum_m (\Omega_m)^2 = \frac{\partial}{\partial X_R}\sum_m (\Omega_m)^2 = 0 \tag{6}$$

As consequence of fitting the Fourier coefficients using a least squares approach, a larger number of wave gauges than unknown parameters are needed, as the reflection analysis benefits from an overdetermined system. The directional analysis in general requires minimum 3 wave gauges. The equations for solving for the two unknown parameters X_I and X_R in Eq. (6) can be written as:

$$\begin{bmatrix} A_{11} & A_{12} \\ A_{21} & A_{22} \end{bmatrix} \begin{bmatrix} X_I \\ X_R \end{bmatrix} = \begin{bmatrix} B_1 \\ B_2 \end{bmatrix} \tag{7}$$

The elements of A_{ij} and B_i are given by:

$$A_{11} = \sum_m \left(C_{I,m}\right)^2$$
$$A_{12} = \sum_m \left(C_{I,m}C_{R,m}\right) = A_{21}$$
$$A_{22} = \sum_m \left(C_{R,m}\right)^2 \tag{8}$$
$$B_1 = \sum_m \left[\hat{\eta}(x_m, y_m)C_{I,m}\right]$$
$$B_2 = \sum_m \left[\hat{\eta}(x_m, y_m)C_{R,m}\right] \tag{9}$$

In order to find the best estimate for the directions θ_I and θ_R the error is initially calculated for a mesh of direction combinations. A range for the incident directions and reflected directions are defined, such that the analysis seeks for incident components in a specified range and for reflected components in another specified range as exemplified in Figure 1. The resolution of the mesh is 2°.

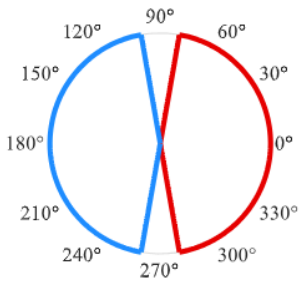

Figure 1. Pre-specified ranges for incident (red) and reflected (blue) wave components.

For each of the given incident and reflected directions of propagation $\theta_I = [\theta_{I,min}; \theta_{I,max}]$ and $\theta_R = [\theta_{R,min}; \theta_{R,max}]$, the linear system of equations in Eq. (7) is solved which yields the isolated complex parameters X_I and X_R with a least-square error, E, determined based on the difference between the estimated and measured Fourier coefficients at all gauge positions as stated in Eq. (5). The computation is repeated for all combinations of directions in the ranges of incident and reflected directions. The combination of directions yielding the lowest error, E, according to the least-squares method is then used as a first estimate. Next, the error, E, is minimised with respect to the incident and reflected directions, θ_I and θ_R, using the Nelder-Mead simplex algorithm (Nelder & Mead, 1965) as implemented in *fminsearch* in MATLAB, from which X_I and X_R in each iteration is calculated by solving the system of equations in Eq. (7). The procedure is repeated for all frequency components.

The incident and reflected wave fields can then be reproduced in time domain in wave gauge position m, or another adjacent position, by Fast Fourier Transform of the decomposed Fourier coefficients stated in Eq. (10) and (11).

$$\hat{\eta}_I(x_m, y_m) = C_{I,m} X_I \tag{10}$$

$$\hat{\eta}_R(x_m, y_m) = C_{R,m} X_R \tag{11}$$

From the decomposed coefficients, the timeseries can also be reproduced from summation as stated in Eq. (2). The amplitudes are then determined as the absolute values of X_I and X_R respectively. The present application uses the *fft* implemented in MATLAB, which yields the phases $\phi = \tan^{-1}\left(\frac{-B}{A}\right)$, where A is the real part of X_I and X_R respectively and B is the imaginary part. The directional spectrum can be estimated following the same procedure as described by Draycott *et al*. (2016).

2.1 Directional settings

During the analysis, the total error, E, is calculated for the full mesh of combinations. An example of how the total error, E, is distributed over the two directions of estimation, θ_I and θ_R, is given in Figure 2 and Figure 3 for an arbitrary frequency component. Figure 2 shows the total error, E, just around the absolute minimum, which is placed at $\theta_I = 23.6°$ and $\theta_R = 223.6°$, where all values of $E > 10^{-6}$ are discarded. To show the full behaviour of the total error, it is shown in logarithmic scale in Figure 3.

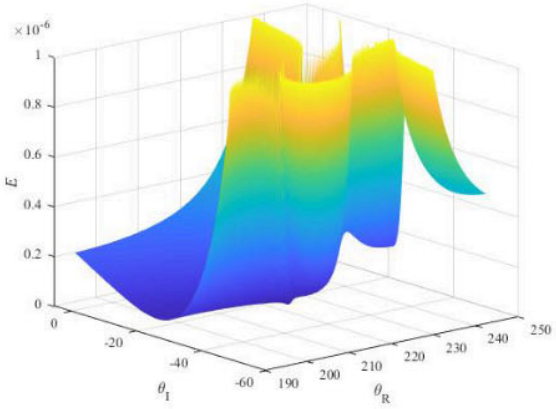

Figure 2. Total error, E, for arbitrary wave component as function of incident, θ_I, and reflected, θ_R, directions. Zoomed in z-axis to show minimum and behaviour around this point.

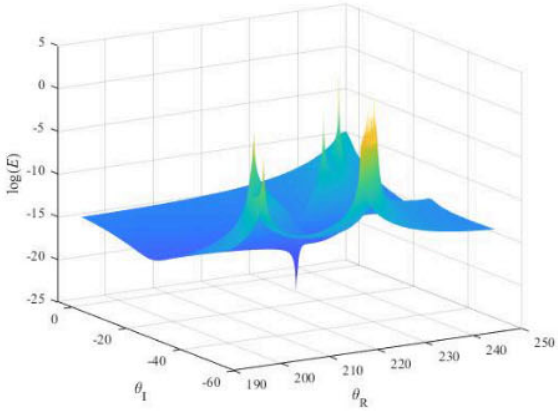

Figure 3. Total error, E, for arbitrary wave component as function of incident, θ_I, and reflected, θ_R, directions. Shown in logarithmic scale for full visualisation of behaviour for a range of directions.

In the process of choosing an appropriate discretisation of the directions, the behaviour of the total error is important to consider. The choice of the discretisation will be a compromise between accuracy of the initial estimates and the computational time. If the discretisation is too coarse, the risk is that local minima will be found in the following optimisation. The consequence of a too coarse grid for the initial mesh is shown in Figure 4, where the estimated reflected direction is seen to be highly influenced by even small errors on the incident direction. In the example studied 30% reflection at angle 223.5° is present in the wave field.

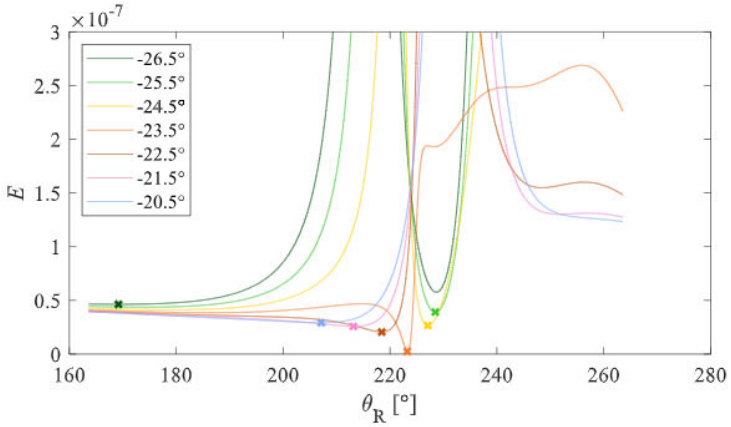

Figure 4. Total error, E, as function of the reflected direction, θ_R, for estimations of the incident direction, θ_I , in the range around the correct value of 23.5°.

Different mesh discretisation for the initial estimates have been investigated through the development of the method, and at present stage 2°-intervals are used as it rarely leads to a local minimum instead of the global to be found.

3 TEST DATA

To test the performance of the SORS decomposition method a series of sea states were generated synthetically. Synthetic data was also used to test sensitivity to deviations from the mathematical model due to wall reflections, noise, calibration errors and errors in position of wave gauges.

3.1 Sea States and Gauge Array

To test the performance of the decomposition method, a set of sea states with different peak periods corresponding to 1:20 scale of a natural environment at the northwestern coast of Denmark is used. The sea states are generated on a water depth h = 0.715 m. All sea states are generated from a JONSWAP spectrum with peak enhancement factor γ = 3.3. The directional parameters of the sea states are defined by the mean wave direction θ_0 and a cos2s spreading function with spreading given by the parameter s. The reflections are given by a reflection coefficient, C_r, and an angle of the reflecting structure, α_s. In the present analyses the structure is placed at a reference point given in x-distance of 6 m from the point of origin (0,0). The wavemakers are placed in line x = 0 m.

An overview of the different sea states and the corresponding significant wave parameters are given in Table 1. The present analyses revolve around waves generated in laboratory facilities, wherefore the frequency span is limited to 0.15 Hz – 3 Hz, which is a typical range of generation in physical model testing. The following analyses will therefore be based on wave gauge measurements of the surface elevation. The present work uses a standard CERC5 wave gauge array as seen in Figure 5, as it is a commonly applied wave gauge array for wave analysis of multidirectional waves, as the internal directions between the gauges are widely spread. The size of the array is adjusted to each sea state, such that the diameter, $D = 2R$, is 0.15 times the wavelength of the peak frequency.

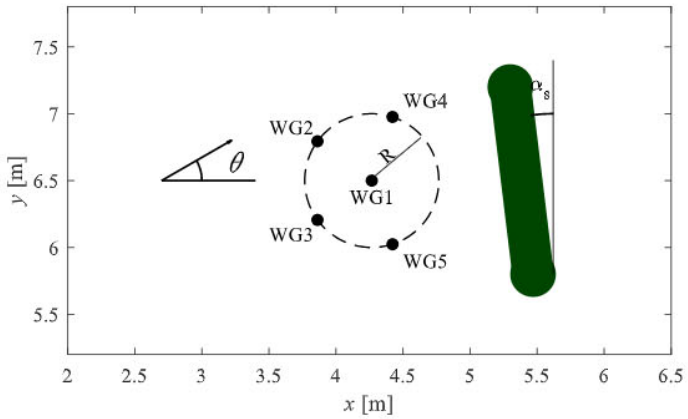

Figure 5. CERC5 wave gauge array.

Table 1. Sea State Parameters.

Sea State	H_{m0} [m]	T_p [s]	θ_0 [°]	s [-]	C_r [-]	α_s [°]
1	0.05	1.25	0	10	0.3	10
2	0.1	1.56	0	10	0.3	10
3	0.15	1.88	0	10	0.3	10
4	0.2	2.19	0	10	0.3	10
5	0.25	2.50	0	10	0.3	10

3.2 Wave Generation

The present work revolves around analysis of multidirectional wave fields generated from the single summation model. This means that each generated frequency component has a single direction. As described in the previous section, the waves with a directional spreading function as suggested by Mitsuyasu *et al*. (1975) will be considered, with the directional spreading function, $D(\theta)$, given in terms of the mean wave direction, θ_0, and spreading parameter, s, as stated in Eq. (12).

$$D(\theta) = \frac{2^{2s-1}\Gamma^2(s+1)}{\pi\Gamma(2s+1)}\cos^{2s}\left(\frac{\theta-\theta_0}{2}\right) \tag{12}$$

Where the double summation generation method would generate several components at the same frequency representing the directional spreading function in Eq. (12), the single summation method assumes only one direction for each frequency component. The individual directions are chosen by Monte Carlo simulation of the probability density function of the directional spreading function, $D(\theta)$. A uniformly distributed random number between 0 and 1 is generated for each frequency. The random number will then represent the non-exceedance probability of the directional distribution function, which will be assigned to the component. The surface elevation, η, in position (x, y) at time t can then be calculated from Inverse Fast Fourier Transform (IFFT) or from summation as described by Eq. (1). The phase of each component (φ_i) is chosen by picking a uniformly distributed random number between $-\pi$ and π. The single summation method accounts for wave generation in physical tank testing as well as generation of synthetic waves. For the synthetic wave fields, which are analysed in the present work, a reflected wave field is similarly generated. The directions and phases of the reflected components are calculated from a specified distance to a reflecting structure with a specified angle. This reproduces thus a wave field with phase locking in front of the structure.

4 RESULTS

The performance of method can be evaluated based on different parameters depending on the desired application of the analysis. For use in physical model testing of offshore structures, the aim is often to validate the generated sea state and its kinematics and correlate it to measured wave loads on the tested model. Therefore, the performance of the method is here evaluated based on how well the incident and reflected timeseries of the surface elevation are reproduced by the method. First, a wave field which fully satisfies the assumptions of the presented method is analysed. Thereafter, the robustness of the method will be demonstrated towards tank testing phenomena such as wall reflections, noise, calibration error, etc.

As the waves of the present analyses are synthetically generated without errors, the target total timeseries are identical with the 'measured' timeseries. An example of the results of the analyses appears in Figure 6, where a segment of the timeseries of the surface elevation in position of WG1, cf. Figure 5, for sea state 1, cf. Table 1, with 30% reflection is shown. Using the presented method, the incident and reflected timeseries are accurately reproduced, with error signals with maximum 0.2% of the variance of the original signal. The combined surface elevation of the incident and reflected wave field are illustrated as the total estimated surface elevation, which is seen to match the 'measured' and, in this case, therefore also the target value accurately.

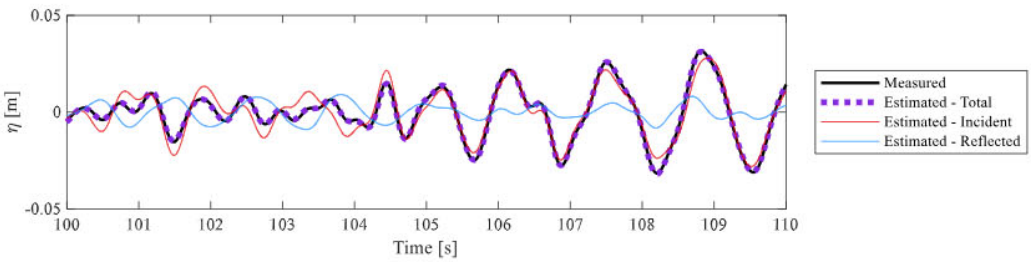

Figure 6. Timeseries of measured surface elevation (here synthetically generated) and result from the analysis, Sea State 1.

The synthetic generation of the waves also allows for a direct compared of the target incident and reflected components

with the prediction by the method. From Figure 7 it is seen that the decomposed timeseries also match the target values very well, with a variance in the error signals relative to the target of 0.04% for the incident and 0.05% for the reflected waves taken as the mean over all gauge positions.

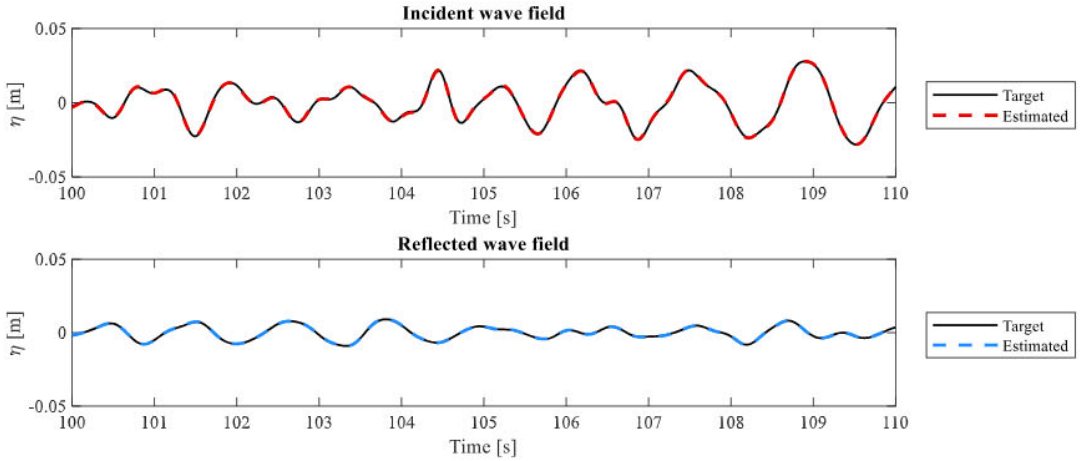

Figure 7. Timeseries of decomposed wave fields compared to the target timeseries, Sea State 1.

As the analysis is performed for all generated frequency components in the spectrum, the values of the individual wave component parameters can also be investigated further. The individual estimated wave component parameters of this specific sea state are compared to the target values as $\Delta\theta = \theta_{est} - \theta_{target}$ for the direction, $\Delta a/a = \left||X_{est}| - |X_{target}|\right| / |X_{target}|$ for the amplitude, $\Delta\phi = \phi_{est} - \phi_{target}$ for the phase and $E_{rel} = \frac{E}{\Sigma_m \hat{\eta}_{target}}$ for a relative estimate of the total error over all gauges compared to the energy of the specific component. The values are calculated for the total, incident and reflected components as relevant. The errors on each frequency component appear from Figure 8.

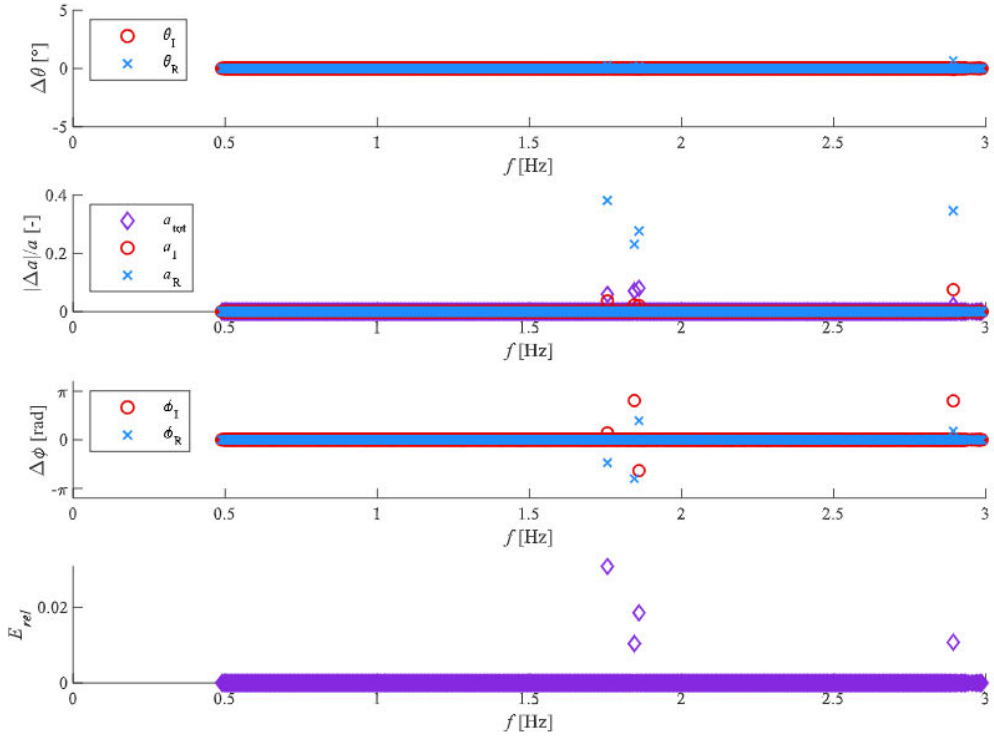

Figure 8. Error on estimated wave component parameters compared to target values for Sea State 1 (f_p = 0.8 Hz).

From Figure 8 it appears that theFigure 8. Error on estimated wave component parameters compared to target values for

Sea State 1 (f_p = 0.8 Hz). accuracy of the estimation is very high. On few high-frequent components, small deviations on the estimated amplitudes and phases are present. One reason for the reduced accuracy of the high frequency components can be the design of the gauge array, as the wavelengths of these components become too small for the present array design.

For in-line reflection analysis, it is recommended, that the wave gauge distances are in the range of 0.05-0.45 times the wavelength as shown by Goda and Suzuki (1976). The distances between the gauges in the present array depend on the direction of propagation of the specific component, wherefore the number of gauge separations that fulfill this requirement will vary with frequency, due to the wavelength, as well as the direction of propagation. The number of valid gauge separations for the CERC5 array given in Figure 5 is illustrated in Figure 9, where the array is scaled to sea state 1, such that the diameter $D = 0.15L_p$, where L_p is the wavelength of the peak frequency, which is the same sea state as the previous results.

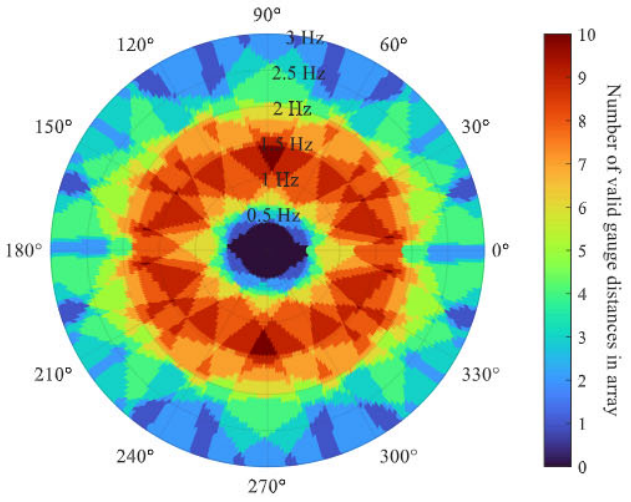

Figure 9. Gauge distances in the CERC5 array scaled to sea state 1, that satisfy the criteria $0.05L < \Delta x_\theta < 0.45L$, where Δx_θ is the distance between two gauges in the direction of propagation of the wave component, illustrated as function of the direction [°] and frequency [Hz].

Another way to determine if the gauge array is useful and an accurate solution to the linear system of equations exists, is based on the condition number as suggested by de Ridder *et al*. (2023). Based on the estimated incident and reflected directions, the condition number is determined as the 2-norm condition number given by Demmel (1987) as the maximal singular value divided by the minimum singular value of the phase difference matrix, Z:

$$Z = \begin{bmatrix} C_{I,1} & C_{R,1} \\ \vdots & \vdots \\ C_{I,m} & C_{R,m} \end{bmatrix} \tag{13}$$

For the same sea state as used in Figure 8, the condition number of the estimated incident and reflected directions for the CERC5 wave gauge array appears from Figure 10 for all frequency components in the analysed spectrum. Similar results are found for the other sea states, indicating that an accurate solution exists for the relevant frequencies and directions for all sea states. Thus, the CERC5 array has a sufficient amount of wave gauges with acceptable distance between them for the present analyses. The layout of the wave gauge array therefore does not yield any limitations to the method. No upper limit, C_{max}, is determined for the present analyses, as it does not seem to increase significantly at any point.

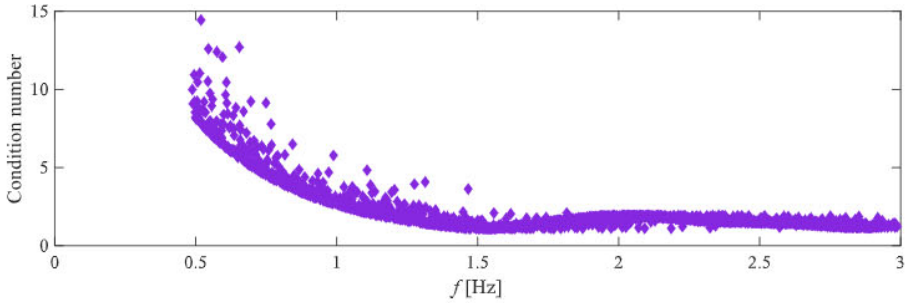

Figure 10. Condition number based on estimated incident and reflected wave directions using the CERC5 array, Sea State 1.

From visual inspection of the timeseries in Figure 6 and Figure 7, the method accurately decomposes wave fields that

strictly follow the assumptions. The performance of the method is further quantified based on the variance of the difference between the estimated surface elevation and the target as stated in Eq. (14). The analyses are performed for all sea states as given in Table 1.

$$\Delta\sigma^2 = \mathrm{Var}(\eta_{est} - \eta_{target}) \tag{14}$$

The results are presented as the average error over all frequencies and all wave gauge positions in Figure 11 and results are summarised in Table 2.

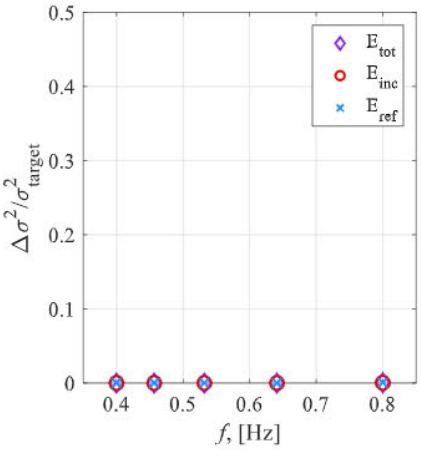

Figure 11. Error on estimated timeseries.

Table 2. Variance error on estimated timeseries compared to target.

Sea State	E_{tot}	E_{inc}	E_{ref}
1	0.04 %	0.04 %	0.05 %
2	0.00 %	0.00 %	0.03 %
3	0.00 %	0.00 %	0.02 %
4	0.00 %	0.00 %	0.03 %
5	0.00 %	0.00 %	0.03 %

From Table 2 it appears that the higher the peak frequency, the higher the error on the timeseries. For the sea states with the higher peak frequency, the wavelengths within for instance half to two times the peak frequency has a larger relative difference than the spectra with the lower frequencies. In such case the size and design of array is of influence despite being scaled in size for each of the sea states in the present analyses.

4.1 Sensitivity to errors

The sensitivity of the method will then be tested towards factors that cause measurements to deviate from the mathematical model in Eq. (2). First, it is tested how additional reflected components, stemming from for instance basin wall reflections behind or beside the structure, more than one model in the basin etc., will affect the decomposition of the wave fields. The same wave fields as the ones given the results in Figure 11 are tested, which means that it includes all five sea states given in Table 1 with 30% reflection. Apart from this, additional 10% reflection from the back wall of the wave tank is included. The back wall of the basin is placed perpendicular to the y-axis 8m from the wavemakers. The results in Figure 12 show the error on the reconstructed timeseries taken as the mean over all wave gauges, where it from the error on the incident wave field, E_{inc}, is seen that the estimation of the incident wave field is almost unaffected by the additional reflected components. E_{ref} is a comparison of the estimated reflected wave field and the target reflected wave field from the structure only, where it is apparent that the estimated reflection is highly affected by an additional wall reflection. The error on the sum of the structure and wall reflection is given by $E_{ref+wall}$ which is seen to be significantly smaller than E_{ref}. For cases where the difference in direction between the wall reflections and reflections from the structure is larger, the error on the reflected wave field is expected to be higher. If the reflection coefficient is larger than in the present example, then an additional reflected direction might also influence the estimated incident direction.

For the sensitivity towards noise, white gaussian noise is added to wave fields with a signal-to-noise ratio of 50:1 of the energy. As seen from Figure 13, the method is fully robust towards noise on the signals when sufficient number of gauges are

applied.

The following part of the sensitivity analysis revolves around measurement errors related to the use of wave gauges in the laboratory facilities. For the sensitivity towards positional error of the wave gauge three different configurations have been tested; one gauge moved 0.03m in the x-direction, one gauge moved 0.03m in the y-direction, and a configuration where one gauge is moved 0.03m in the x-direction and another gauge is moved 0.03m in the y-direction. These results appear from Figure 14, where it is seen that the method is very robust towards small inaccuracies in position of the wave gauges. The incident wave field is almost unaffected by the positional error, possibly due to the relatively larger amount of energy, whereas a small increase in the error is seen on the reflected part of the spectrum. Furthermore, the behaviour of the error as function of the frequency is more like the general pattern seen for the full spectrum analyses in Figure 11, that the larger the peak frequency, the lower accuracy is experienced.

Another type of measurement error could be calibration errors. Two different configurations of possible calibration errors are tested; 10% gain on one gauge, and 10% gain on one gauge with -10% on another gauge. The results appear from Figure 15. As the analysed wave fields contain 30% reflection, it is natural that the relative error on the reflected wave field is larger than on the incident wave field. Overall, it can be concluded, that the calibration errors can be rather critical for estimation of the reflected wave field, but less critical for the incident components, which are of primary interest. This conclusion might be different if more gauges were affected by calibration errors.

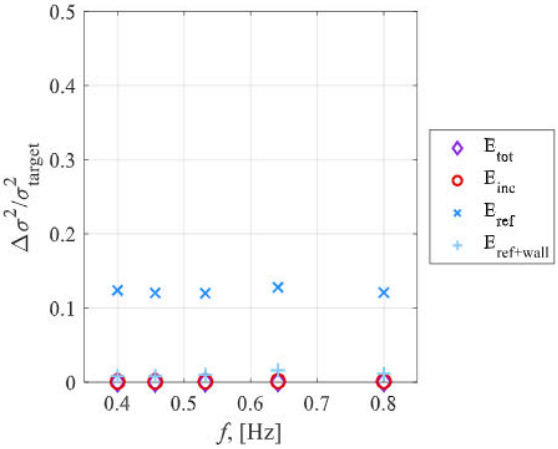

Figure 12. Error on estimated timeseries, wall reflection.

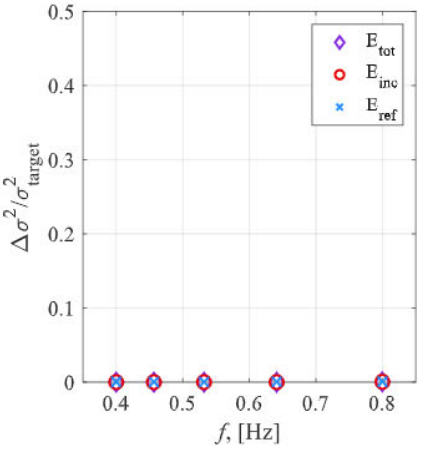

Figure 13. Error on estimated timeseries, noise.

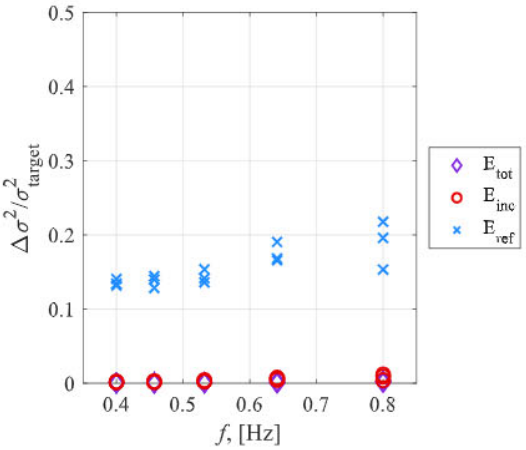

Figure 14. Error on estimated timeseries, wave gauge position error.

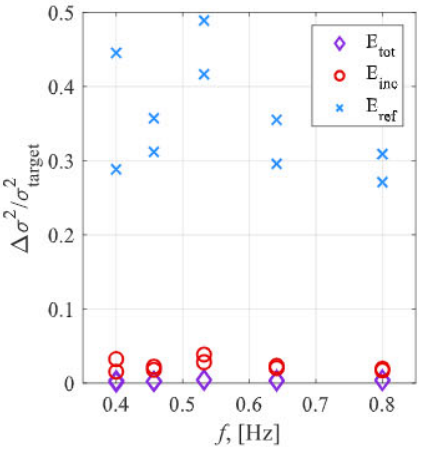

Figure 15. Error on estimated timeseries, wave gauge calibration error.

5 DISCUSSION

The method is structured in the way that a first estimate of the incident and reflected components of each frequency component is calculated from a mesh of different directions, wherefrom the combination yielding the lowest total error on the Fourier coefficients is chosen as initial estimates. The mesh is defined based on ranges for the incident and the reflected directions to be defined in agreement with the test conditions. A small gap between the incident and reflected sectors must be present for stability of the method. The size of this gap has in the present partly been based on the condition number. In Figure 16 the condition number with respect to the reflected wave direction θ_R for an incident wave direction of $\theta_I = 0°$ is illustrated. As seen from Figure 16, the condition number increases significantly when the two angles are close to each other, indicating that no accurate solution of the wave decomposition exists. Therefore, the initial ranges of the incident and reflected from Figure 1 are chosen such that a gap of 20 degrees exist between them. The size of this gap may also be chosen frequency dependent to account for the frequency dependency of the condition number shown in Figure 14. This is mainly relevant if a very wide spreading of the waves is present. As it is unlikely that the incident and reflected wave components travel in almost the same direction it does not immediately affect the present implementation of the method.

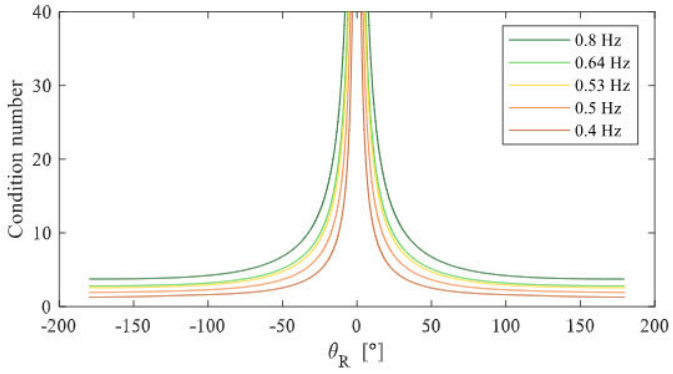

Figure 16. Condition number for CERC5 array as function of reflected direction of propagation θ_R for incident wave direction $\theta_I = 0°$ for relevant frequencies corresponding to peak frequencies of the investigated sea states.

In general, Wenneker and Hofland (2014) suggests using the condition number to design the gauge array. However, the design process is not as straightforward when dealing with multidirectional waves, which is also supported by Figure 9, where the directional variation of the valid gauge distances appears. Gauge array design for decomposition of multidirectional waves should therefore be investigated further. The gauge array for analysis of multidirectional waves is often designed based on the co-array or lag-array, which describes the internal distances of the wave gauges (Haubrich (1968), Davis and Regier (1977)), for which the considerations regarding reflection analysis is however not included.

5.1 Future work

As mentioned earlier, further work should include a more detailed design of the wave gauge array for decomposition of multidirectional waves using the present method. Further analysis related to the sensitivity towards calibration errors should investigate the effects from truncation of the spectrum, scaling of the wave gauge array and number of wave gauges applied. Also, an extension for cross-mode identification could be relevant. Apart from that, the sensitivity of the method towards nonlinear effects should be tested. It is expected that the method will behave similarly as other methods when used for analyses of nonlinear wave fields as shown in Iversen *et al.* (2023). The structure of the presented method will allow for implementation of nonlinear effects as done by Eldrup and Andersen (2019), which will however require further work regarding assumptions about the directionality of the nonlinear components to avoid a drastic increase in computational consumption.

6 CONCLUSIONS

For physical model testing of coastal and offshore structure exposed to multidirectional waves, identification of the incident wave field is often required to validate if the sea state matches the target conditions. Most existing methods assume double summation sea states and only provide the directional spectrum and not the time domain parameters. The present paper presents a new methodology for wave decomposition of multidirectional waves generated from the single summation method. The new SORS method successfully reconstructs the incident and reflected wave fields in the time domain. The method allows for oblique reflections, which is not yet covered by existing similar methods for single summation sea states. Through analysis of synthetically generated waves, the SORS method is proven to be robust towards noise, wave gauge calibration errors, positional errors of wave gauges, and additional directional components caused by for example basin wall reflections. The performance of the method in nonlinear waves and potential extension of the method to account for this will be investigated in future work.

ACKNOWLEDGEMENT

This work was funded by the Danish Energy Agency under The Energy Technology Development and Demonstration Program (EUDP) contract number 64022-1062.

REFERENCES

Capon, J., Greenfield, R. J., & Kolker, R. J. (1976). Multidimensional maximum-likelihood processing of a large aperture seismic array. *Proc. IEEE*, 55, 192-211.

Dalrymple, R. A. (1989). Directional wavemaker theory with sidewall reflection. *Journal of Hydraulic Research*, 27:1, 23-34.

Davis, R. E., & Regier, L. A. (1977). Methods for estimating directional wave spectra from multi-element arrays. *Journal of Marine Research*, 35 (3), 453-477.

de Ridder, M. P., Kramer, J., den Bieman, J. P., & Wenneker, I. (2023). Validation and practical application of nonlinear wave decomposition methods for irregular waves. *Coastal Engineering*, 183, 104311.

Demmel, J. W. (1987). On condition numbers and the distance to the nearest ill-posed problem. *Numerische Mathematik*, 51, 251-289.

Draycott, S., Davey, T., Ingram, D. M., Day, A., & Johanning, L. (2016). The SPAIR method: Isolating incident and reflected directional wave spectra in multidirectional wave basins. *Coastal Engineering*, 114, 265-283.

Eldrup, M. R., & Andersen, T. L. (2019). Estimation of Incident and Reflected Wave Trains in Highly Nonlinear Two-Dimensional Irregular Waves. *Journal of Waterway, Port, Coastal and Ocean Engineering*, 145(1).

Goda, Y., & Suzuki, T. (1976). Estimation of incident and reflected waves in random wave experiments. *Proceedings of the 15th Coastal Engineering Conference*, 828-845.

Hashimoto, N., & Kobune, K. (1988). Directional spectrum estimation from a Bayesian Approach. *Coastal Engineering Proceedings*, 62-76.

Hashimoto, N., Nagai, T., & Asai, T. (1994). Extension of the maximum entropy principle method for directional wave spectrum estimation. *Coastal Engineering Proceedings*, 232-246.

Haubrich, R. A. (1968). Array Design. *Bulletin of the Seismological Society of America*, 58 (3), 977-991 .

Hawkes, P. J., Ewing, J. A., Harford, C. M., Klopman, G., Stansberg, C. T., Benoit, M., . . . Schäffer, H. A. (1997). Comparative Analysis of Multidirectional Wave Basin Data. *IAHR Seminar on Multidirectional Waves and their Interaction with Structures*.

Isobe, M., Kondo, K., & Horikawa, K. (1984). Extension of mlm for estimating directional wave spectrum. *Proc. Sympo. On Description and Modelling of Directional Seas*, A-6.

Iversen, S. K., Andersen, T. L., & Frigaard, P. (2023). Accuracy of Directional Spectrum Estimation in 2nd Order Multidirectional Waves. *Proceedings of the Thirty-third International Ocean and Polar Engineering Conference*, Ottawa, Canada, 2395-2402.

Krogstad, H. E. (1988). Maximum likelihood estimation of ocean wave spectra from general arrays of wave gauges. *Modelling, Identification and Control*, 9, 373-381.

Mansard, E. P., & Funke, E. R. (1980). The measurement of incident and reflected spectra using a least squares method. *Proceedings of the 17th Coastal Engineering Conference*, 154-172.

Miles, M. D., & Funke, E. R. (1989). A comparison of methods for synthesis of directional seas. *Journal of Offshore Mechanics and Arctic Engineering*, 111, 43-48.

Mitsuyasu, H., Tasai, F., Suhara, T., Mizuno, S., Onkusu, M., Honda, T., & Rukiiski, K. (1975). Observations of the directional spectrum of ocean waves using a cloverleaf buoy. *J. Phys. Oceanogr.*, 5, 751-761.

Nelder, J. A., & Mead, R. (1965). A Simplex Method for Function Minimization. *The Computer Journal*, 7, 4, 308-313.

Wenneker, I., & Hofland, B. (2014). Optimal wave gauge spacings for separation of incoming and reflected waves. *Proceedings on the Fifth International Conference on the Application of Physical Modelling to Port and Coastal Protection (Coastlab)*.

Zelt, J. A., & Skjelbreia, J. E. (1993). Estimating Incident and Reflected Wave Fields Using an Arbitrary Number of Wave Gauges. *Coastal Engineering*, 777-789.